

## Angle-dependent sound absorption estimation using a compact microphone array

Mansour Alkmim, Jacques Cuenca, Laurent De Ryck, et al.

Citation: *The Journal of the Acoustical Society of America* **150**, 2388 (2021); doi: 10.1121/10.0006566

View online: <https://doi.org/10.1121/10.0006566>

View Table of Contents: <https://asa.scitation.org/toc/jas/150/4>

Published by the *Acoustical Society of America*

---

### ARTICLES YOU MAY BE INTERESTED IN

[Improved accuracy for radiation damping in coupled finite element/equivalent source computations](#)

*The Journal of the Acoustical Society of America* **150**, 2375 (2021); <https://doi.org/10.1121/10.0006414>

[Automated partial differential equation identification](#)

*The Journal of the Acoustical Society of America* **150**, 2364 (2021); <https://doi.org/10.1121/10.0006444>

[Toward a physical model of the clavichord](#)

*The Journal of the Acoustical Society of America* **150**, 2350 (2021); <https://doi.org/10.1121/10.0006438>

[In situ characterization of laser-generated melt pools using synchronized ultrasound and high-speed X-ray imaging](#)

*The Journal of the Acoustical Society of America* **150**, 2409 (2021); <https://doi.org/10.1121/10.0006386>

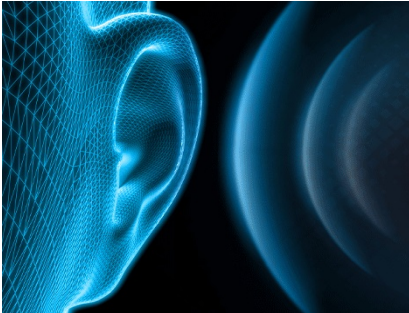
[Acoustic differences between Chilean and Salvadoran Spanish /s/](#)

*The Journal of the Acoustical Society of America* **150**, 2446 (2021); <https://doi.org/10.1121/10.0006443>

[Three-dimensional spiral motion of microparticles by a binary-phase logarithmic-spiral zone plate](#)

*The Journal of the Acoustical Society of America* **150**, 2401 (2021); <https://doi.org/10.1121/10.0006417>

---



**JASA**  
THE JOURNAL OF THE  
ACOUSTICAL SOCIETY OF AMERICA

**SPECIAL ISSUE:**  
Noise-Induced Hearing Disorders:  
Clinical and Investigational Tools

**SUBMIT TODAY!**

## Angle-dependent sound absorption estimation using a compact microphone array

Mansour Alkmim,<sup>1,a)</sup> Jacques Cuenca,<sup>1</sup> Laurent De Ryck,<sup>1</sup> and Wim Desmet<sup>2,b)</sup>

<sup>1</sup>Siemens Digital Industries Software, Interleuvenlaan 68, B-3001 Leuven, Belgium

<sup>2</sup>Department of Mechanical Engineering, KU Leuven, Celestijnenlaan 300 B, B-3001, Leuven, Belgium

### ABSTRACT:

This paper proposes a method for estimating the angle-dependent sound absorption coefficient of a large material sample using a compact microphone array. The method relies on the description of the pressure field as a pair of in-going and out-going waves or using an image source model and stands as a generalization of the classical two-microphone method. The array includes an irregular spacing normal to the surface to avoid spatial aliasing. Furthermore, the benefit of additional microphones parallel to the sample is investigated, while keeping the array compact. The approach is validated against the transfer matrix method as well as against locally and non-locally reactive surface models and compared to the two-microphone method. The sensitivity of the estimation to uncertainties in the microphone positions is evaluated by means of a Monte Carlo approach. Measurements above melamine foam and gravel samples are presented and illustrate the reduced uncertainty in the sound absorption estimation. In particular, the proposed method exhibits improved robustness compared to the two-microphone method, especially at low frequencies.

© 2021 Author(s). All article content, except where otherwise noted, is licensed under a Creative Commons Attribution (CC BY) license (<http://creativecommons.org/licenses/by/4.0/>). <https://doi.org/10.1121/10.0006566>

(Received 4 November 2020; revised 14 September 2021; accepted 17 September 2021; published online 5 October 2021)

[Editor: Jordan Cheer]

Pages: 2388–2400

### I. INTRODUCTION

The random- and normal-incidence sound absorption coefficients are among the most commonly used metrics to acoustically characterize materials. Internationally standardized methods exist for the measurement of normal and random incidence sound absorption (ISO, 2003; ISO, 1998). However, such sound absorption coefficients are known to provide limited information on the acoustic behavior of materials (Bezemer-Krijnen *et al.*, 2014; Dupont *et al.*, 2020; Hald *et al.*, 2019; Ottink *et al.*, 2016; Rathsam and Rafaely, 2015; Richard *et al.*, 2017; Robin *et al.*, 2014). Indeed, the acoustic reflection and absorption characteristics of non-homogeneous or non-locally reactive materials can vary depending on the sound source incidence angle and distance. As such, the study of angle-dependent sound absorption coefficients is crucial for a wide range of applications, e.g., realistic room acoustic simulations with moving sources, outdoor ground impedance measurements, and sound synthesis of pass-by noise. Particularly, to predict the noise emissions at the early stages of vehicle design, new tools for sound synthesis of moving sources are being developed (Alkmim *et al.*, 2020). According to the ISO standard for the pass-by noise test (ISO, 2015), at normal incidence, the sound absorption coefficient of the asphalt layer has to be below

8% (ISO, 2014). However, the sound absorption coefficient estimation is commonly performed using vertical impedance tubes which only provide the normal incidence acoustic characteristics of the asphalt and do not give information of the local or non-local reaction characteristics of the material.

Techniques for the estimation of the oblique-incidence sound absorption coefficient can be found as an alternative to standard laboratory procedures. These approaches are based on the separation of reflected and incident components using elementary wave functions (i.e., spherical or plane) (Hald, 2009; Nolan, 2020; Tamura, 1990). Alternatively, reconstruction methods use the obtained wave decomposition to calculate the sound pressure and particle velocity on the surface of the material (Hald *et al.*, 2019; Richard and Fernandez-Grande, 2019; Richard *et al.*, 2017). With direct application to *in situ* acoustic characterization of porous asphalt, Bezemer-Krijnen *et al.* (2014) presented a measurement technique to obtain the oblique-incidence sound absorption coefficient based on the local specular plane wave assumption. The measurement device therein uses an 8-microphone cubic array. In their approach, the source location was assumed to be unknown, thus requiring a minimization strategy to retrieve its position. The uncertainty of the retrieved angle of incidence of this approach was about 10° and the method showed a large standard deviation, especially at lower frequencies. In terms of array geometry, irregular spacing of the microphones in the direction normal to the surface of interest is known to mitigate aliasing errors, especially at high frequencies (Cuenca and De Ryck, 2015; Nolan, 2020).

<sup>a)</sup>Also at: KU Leuven, Department of Mechanical Engineering, Celestijnenlaan 300 B, B-3001, Leuven, Belgium. Electronic mail: mansour.alkmim@siemens.com, ORCID: 0000-0003-3416-4401.

<sup>b)</sup>Also at: DMMS core lab, Flanders Make, Gaston Geenslaan 8, 3001 Heverlee, Belgium.

This paper proposes a method for estimating the angle-dependent sound absorption coefficient using a compact microphone array setup. The method relies on a wave splitting (WS) technique where the acoustic field is modeled as a superposition of incident and reflected plane waves above an infinite plane and assuming specular reflection. Alternatively, the acoustic field is modeled using the image source method (ISM). The appropriate choice of the acoustic model, which depends on the measurement conditions, is investigated using analytical pressure field models as a reference. The WS approach, described in this paper, is similar to that in [Bezemer-Krijnen et al. \(2014\)](#) with the main difference being that the source position is assumed to be known *a priori*, hence, not requiring an optimization procedure. The novelty of the work lies in the use of an irregularly-spaced microphone array with the additional constraint of the latter being compact for portability, in particular for *in situ* applications. The method presented in this paper attempts to improve broadband estimation with respect to the classical two-microphone method, for instance. The method is suitable for the *in situ* acoustic characterization of sufficiently large planar surfaces for which sample size effects occur at frequencies below the range of interest. In this paper, this effect is not accounted for in the sound absorption estimation.

The paper is structured as follows: Sec. II introduces the analytical pressure field models used as the target for the validation of the proposed method. The latter is detailed in Sec. III, where both wave-splitting and image source representations are used. Numerical validation results are presented in Sec. IV and experimental results for a melamine foam and a gravel sample are shown in Sec. V.

## II. FORWARD MODELS

As a basis to validate the approach proposed in this paper, analytical pressure field models are here considered. Three models are used, a single-layer transfer matrix model (TMM) as a reference and two full-field models for a point source above the surface of interest. The material is modeled as an equivalent fluid whose effective density and characteristic impedance derive from the Johnson-Champoux-Allard (JCA) model ([Champoux and Allard, 1991](#); [Johnson et al., 1987](#)). Time dependency is assumed to be  $e^{j\omega t}$ , where  $j$  is the imaginary unit,  $\omega$  is the angular frequency, and  $t$  is time and is implicit throughout the paper.

### A. TMM

The theoretical predictions of the sound absorption coefficient are derived from the transfer matrix method. The TMM assumes a plane wave pressure field and a single layer backed by a fully rigid wall. The angle-dependent absorption coefficient is expressed as ([Allard, 1993](#))

$$\alpha_{\text{TMM}}(\theta, \omega) = 1 - \left| \frac{Z_s \cos(\theta) - \rho_0 c_0}{Z_s \cos(\theta) + \rho_0 c_0} \right|^2, \quad (1)$$

where  $\rho_0$  and  $c_0$  are the air density and speed of sound, respectively, and  $Z_s$  is the surface impedance, given by

$$Z_s = -jZ_c \frac{k_m}{k_{m,z}} \cot(k_{m,z}d), \quad (2)$$

where  $k_m$  and  $k_{m,z}$  are the porous layer wavenumber and its component on the  $z$ -axis, respectively;  $Z_c$  is the characteristic impedance of the porous layer. Note that Eq. (2) represents a surface impedance with non-locally reactive assumption. When  $k_{m,z} = k_m$ , Eq. (2) represents a normal incidence condition and the surface impedance is equivalent to that predicted by a locally-reactive assumption. These two models are used here, denoted TMM non-locally reactive (NLR) for the non-locally reactive assumption and TMM locally-reacting (LR) for the locally reactive assumption.

### B. Di and Gilbert model: Pressure field above surfaces with local reaction assumption

The [Di and Gilbert \(1993\)](#) model assumes a frequency-dependent LR surface impedance and the sound pressure is given by

$$p(\mathbf{r}) = \frac{e^{-jk_0|\mathbf{r}-\mathbf{r}_s|}}{|\mathbf{r}-\mathbf{r}_s|} + \frac{e^{-jk_0|\mathbf{r}-\mathbf{r}_{is}|}}{|\mathbf{r}-\mathbf{r}_{is}|} - 2k_0\beta \int_0^\infty \frac{e^{-k_0\beta q} e^{-jk_0\sqrt{r^2+(z_s+z-jq)^2}}}{\sqrt{r^2+(z_s+z-jq)^2}} dq, \quad (3)$$

where  $|\mathbf{r}-\mathbf{r}_s| = \sqrt{(x-x_s)^2 + (y-y_s)^2 + (z_s-z)^2}$  and  $|\mathbf{r}-\mathbf{r}_{is}| = \sqrt{(x-x_s)^2 + (y-y_s)^2 + (z_s+z)^2}$  are the Euclidean distances from the receiver  $\mathbf{r}$  to the source  $\mathbf{r}_s$  and image source  $\mathbf{r}_{is}$ , respectively;  $r = \sqrt{(x-x_s)^2 + (y-y_s)^2}$  is the source-receiver distance in the  $(x, y)$  plane. The porous material is classically represented by its normalized admittance in the form  $\beta = (\rho_0 c_0)/Z_s$  and  $k_0$  is the wavenumber in air.

### C. Allard et al. model: Pressure field above surfaces with non-local reaction assumption

The [Allard et al. \(1992\)](#) model assumes a NLR rigid-backed porous material, and the sound pressure is given by

$$p(\mathbf{r}) = \frac{e^{-jk_0|\mathbf{r}-\mathbf{r}_s|}}{|\mathbf{r}-\mathbf{r}_s|} - \frac{e^{-jk_0|\mathbf{r}-\mathbf{r}_{is}|}}{|\mathbf{r}-\mathbf{r}_{is}|} + \int_0^\infty \frac{2\rho_m e^{-v_0|z_s+z|}}{v_0\rho_m + v_m\rho_0 \tanh(v_m d)} sJ_0(sr) ds, \quad (4)$$

where  $\rho_m$  is the equivalent effective density of the porous layer,  $d$  is the thickness of the porous layer,  $J_0$  is the zero-order Bessel function of the first kind,  $v_0 = \sqrt{s^2 - k_0^2}$ , and  $v_m = \sqrt{s^2 - k_m^2}$ . Note that the effect of the porous material is included in the pressure field expression through its acoustic properties  $\rho_m$  and  $k_m$ , whereas in Eq. (3), the porous layer is accounted for by the normalized admittance at normal incidence.

### III. SOUND ABSORPTION ESTIMATION

The proposed methodology is based on the linear inversion of a propagation matrix. Assuming that the incident and the reflected fields can be described as either plane or spherical waves, two methods are used, respectively, a WS approach and an ISM. The choice of the elementary description of the pressure field is made due to the limited number of measurement points, which is imposed as a design constraint.

#### A. Estimation of surface sound absorption using a compact microphone array

Consider the sound pressure field at any point with  $z > 0$ , i.e., above the surface of interest as shown in Fig. 1.

For a discrete set of  $Q$  microphones above an infinite surface, the pressure field for each microphone can be described by a system of linear equations, written in matrix form (Cuenca and De Ryck, 2015; Wang and Chen, 2018)

$$\mathbf{p} = \mathbf{E}\mathbf{w}, \tag{5}$$

where  $\mathbf{w}(\mathbf{r}_s, \omega) = [w_{\text{in}}(\mathbf{r}_s, \omega) \ w_{\text{out}}(\mathbf{r}_s, \omega)]^T \in \mathbb{C}^2$  is the vector of discrete complex amplitudes for the incident and specular reflected components, respectively;  $\mathbf{p}(\omega) = [p(\mathbf{r}_1) \ p(\mathbf{r}_2) \ \dots \ p(\mathbf{r}_Q)]^T \in \mathbb{C}^{Q \times 1}$  is the vector of the acoustic pressure at the  $Q$  microphones, and  $\mathbf{E} \in \mathbb{C}^{Q \times 2}$  is the wave propagation matrix.

For a microphone array with more than two microphones (i.e.,  $Q > 2$ ) the system provides more data than there are unknowns and, in general, does not yield an exact solution. To find an approximate solution, the system of

equations can be solved in a least squares sense, for instance by employing the Moore-Penrose pseudo-inverse, as

$$\mathbf{w} = \mathbf{E}^\dagger \mathbf{p}, \tag{6}$$

where  $\mathbf{E}^\dagger = (\mathbf{E}^T \mathbf{E})^{-1} \mathbf{E}^T$  is the left pseudo-inverse of  $\mathbf{E}$ . However, the condition  $Q > 2$  does not guarantee that the system is over-determined, especially for large wavelengths, where phase differences between microphones are small. In addition, the presence of noise and errors in the model representation of the real acoustic field distribution can contribute to the ill-conditioning of the inverse problem (Kim and Nelson, 2004; Nelson and Yoon, 2000). Therefore, regularization approaches are employed, commonly, in the form of Tikhonov regularization  $\mathbf{w} = (\mathbf{E}^T \mathbf{E} + \lambda \mathbf{I})^{-1} \mathbf{E}^T \mathbf{p}$ , where  $\mathbf{I}$  is the identity matrix and  $\lambda$  is the regularization parameter that can be appropriately chosen using, for instance, the L-curve or generalized cross-validation methods (Hansen, 1994).

In the case of a pressure field assuming the WS into a specular pair of in-going and out-going propagating waves as illustrated in Fig. 1(a), the wave propagation matrix  $\mathbf{E} = \mathbf{E}_{\text{WS}}$ , is given by

$$\mathbf{E}_{\text{WS}} = \begin{bmatrix} e^{-jk_{\text{in}} \cdot \mathbf{r}_1} & e^{-jk_{\text{out}} \cdot \mathbf{r}_1} \\ \vdots & \vdots \\ e^{-jk_{\text{in}} \cdot \mathbf{r}_Q} & e^{-jk_{\text{out}} \cdot \mathbf{r}_Q} \end{bmatrix}, \tag{7}$$

where  $\mathbf{r}_i$ ,  $i = 1, 2, \dots, Q$  are the coordinates of the  $i$ th sensor, and  $\mathbf{k}_{\text{in}} = \mathbf{k}(\theta)$  and  $\mathbf{k}_{\text{out}} = \mathbf{k}(-\theta)$  are the in-going and out-going wavenumbers, respectively.

The components of the wavenumber vector  $\mathbf{k} = (k_x, k_y, k_z)$  satisfy the relation  $k_0 = \sqrt{k_x^2 + k_y^2 + k_z^2}$ . The direction described by  $\mathbf{k}(\theta) = [0 \ k_0 \sin \theta \ k_0 \cos \theta]^T$  is that of the angle of incidence  $\theta$  with respect to the normal to the surface.

In this special case of a plane wave propagation matrix, the angle of incidence fully describes the source position. Hence, the sound absorption coefficient provided by plane WS is given by

$$\alpha_{\text{WS}}(\theta, \omega) = 1 - \left| \frac{w_{\text{out}}(\theta, \omega)}{w_{\text{in}}(\theta, \omega)} \right|^2, \tag{8}$$

where the ratio of the complex wave amplitudes  $w_{\text{out}}(\theta, \omega)/w_{\text{in}}(\theta, \omega)$  is the complex reflection coefficient at incident angle  $\theta$ .

The derivation of the pressure field assuming an ISM as illustrated in Fig. 1(b) assumes a propagation matrix  $\mathbf{E} = \mathbf{E}_{\text{ISM}}$  in the form

$$\mathbf{E}_{\text{ISM}} = \begin{bmatrix} \frac{e^{-jk_0|\mathbf{r}_1 - \mathbf{r}_s|}}{|\mathbf{r}_1 - \mathbf{r}_s|} & \frac{e^{-jk_0|\mathbf{r}_1 - \mathbf{r}_{\text{is}}|}}{|\mathbf{r}_1 - \mathbf{r}_{\text{is}}|} \\ \vdots & \vdots \\ \frac{e^{-jk_0|\mathbf{r}_Q - \mathbf{r}_s|}}{|\mathbf{r}_Q - \mathbf{r}_s|} & \frac{e^{-jk_0|\mathbf{r}_Q - \mathbf{r}_{\text{is}}|}}{|\mathbf{r}_Q - \mathbf{r}_{\text{is}}|} \end{bmatrix}, \tag{9}$$

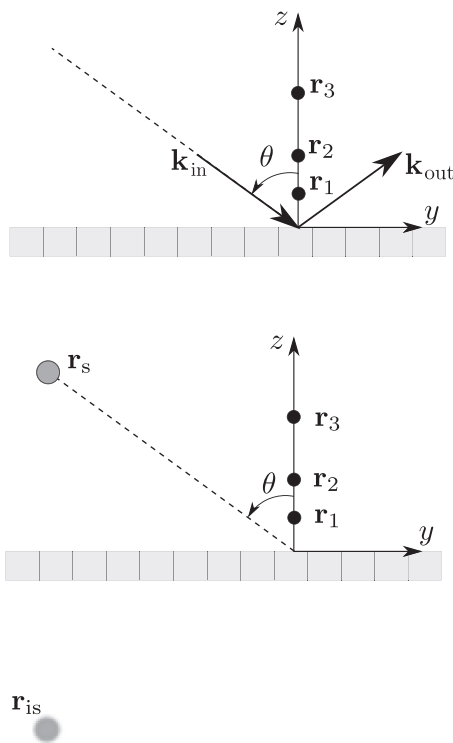


FIG. 1. Cartesian coordinate system defined on the infinite surface of the material with source and receivers in the  $x = 0$  plane for (top) the WS technique and (bottom) the ISM.

where  $\mathbf{r}$  and  $\mathbf{r}_{is}$  are the source and image source coordinates, respectively.

Finally, the sound absorption coefficient of the surface at oblique incidence is defined as

$$\alpha_{ISM}(\mathbf{r}_s, \omega) = 1 - \left| \frac{w_{out}(\mathbf{r}_s, \omega)}{w_{in}(\mathbf{r}_s, \omega)} \right|^2. \quad (10)$$

Note that, in this formulation, it is assumed that the incident and reflected waves are spherical and the term inside the modulus represents the plane wave reflection coefficient due to spherical wavefronts. This approximation has been widely used in the literature (Brandão *et al.*, 2015; Dupont *et al.*, 2020; Richard *et al.*, 2017).

It is worth noting that the WS technique requires the knowledge of the angle of incidence, whereas the ISM requires knowledge of the angle of incidence and range.

However, at large source-receiver distances such that  $|\mathbf{r} - \mathbf{r}_s| \approx |\mathbf{r}_s|$ , the image source model may be approximated by a plane wave model and therefore the two formulations become equivalent for practical purposes. Indeed, the choice of propagation model depends on the nature of the sound field (Richard *et al.*, 2017).

The simplified models in Eqs. (7) and (9) do not account for the complex behavior represented by the third term of Eqs. (3) or (4). Therefore, the proposed estimation procedure provides the pair of plane waves, or point sources, that best approximates the sound field.

### B. Two-microphone method

For the purposes of the present paper, the above sound absorption estimation procedure is compared to the classical two-microphone method (2MM) (Allard and Champoux, 1989). The latter is widely used thanks to its straightforward implementation and experimental setup. The 2MM is a special case of the above sound absorption retrieval procedure based on the ISM, with  $Q = 2$ . The sound absorption coefficient is obtained as

$$\alpha_{2MM}(\mathbf{r}_s, \omega) = 1 - \left| \frac{\frac{e^{-jk_0|\mathbf{r}_1 - \mathbf{r}_s|}}{|\mathbf{r}_1 - \mathbf{r}_s|} \frac{p(\mathbf{r}_1) e^{-jk_0|\mathbf{r}_2 - \mathbf{r}_s|}}{p(\mathbf{r}_2) |\mathbf{r}_2 - \mathbf{r}_s|}}{\frac{e^{-jk_0|\mathbf{r}_2 - \mathbf{r}_{is}|}}{|\mathbf{r}_2 - \mathbf{r}_{is}|} \frac{p(\mathbf{r}_1)}{|\mathbf{r}_1 - \mathbf{r}_{is}|} - \frac{e^{-jk_0|\mathbf{r}_1 - \mathbf{r}_{is}|}}{|\mathbf{r}_1 - \mathbf{r}_{is}|} \frac{p(\mathbf{r}_2)}{|\mathbf{r}_2 - \mathbf{r}_{is}|}} \right|^2, \quad (11)$$

where  $p(\mathbf{r}_1)$  and  $p(\mathbf{r}_2)$  are the pressure field at the two microphones placed at  $\mathbf{r}_1$  and  $\mathbf{r}_2$ , respectively, as described in Fig. 1.

## IV. NUMERICAL VALIDATION

In this section, the WS and ISM are investigated numerically at various angles of incidence and source heights above a melamine foam sample. The methods are compared with the intrinsic sound absorption coefficient obtained from the TMM assuming locally reactive and non-locally reactive surfaces. In Sec. IV A, a two-microphone configuration is considered in order to evaluate the effect of

the plane- and spherical-wave approximations on the sound absorption retrieval. In Sec. IV B, the sensitivity of the proposed method to uncertainty in the positions of the microphones is investigated for three array configurations with a varying number of microphones along the  $y$ -axis.

The equivalent fluid parameters of the material used for the validation are as follows: porosity  $\phi = 0.99$ , flow resistivity  $\sigma = 14\,000 \text{ Pa} \cdot \text{s} \cdot \text{m}^{-2}$ , tortuosity  $\alpha_\infty = 1.01$ , viscous characteristic length  $\Lambda = 80 \mu\text{m}$ , thermal characteristic length  $\Lambda' = 250 \mu\text{m}$  and thickness  $d = 0.03 \text{ m}$ . The parameters are obtained using the measured normal incidence sound absorption coefficient from Sec. V B through an inverse estimation technique (Cuenca and De Ryck, 2015).

### A. Validity of the plane- and spherical-wave approximations

The purpose of this subsection is to evaluate the limitations of approximating the sound pressure field as a pair of plane or spherical waves. For simplicity, a two-microphone configuration is used, that is, using the sound absorption retrieval described in Sec. III A, with  $Q = 2$ . For this configuration, the microphone coordinates are  $\mathbf{r}_1 = (0, 0, 0.018) \text{ m}$  and  $\mathbf{r}_2 = (0, 0, 0.038) \text{ m}$ .

With the aim of evaluating the limits of the plane wave assumption in the WS technique, Fig. 2 shows the sound absorption coefficient at two angles of incidence and for two source positions:  $(0, 10 \sin \theta, 10 \cos \theta) \text{ m}$  and  $(0, 0.7 \sin \theta, 0.7 \cos \theta) \text{ m}$ . The sound field is modeled using the Di and Gilbert (1993) and Allard *et al.* (1992) pressure field models described in Sec. IIB and Sec. IIC, respectively, from which the sound absorption coefficient is estimated using the WS technique.

Figure 2 shows that the plane wave assumption is valid for large source-receiver distances or high frequencies. In particular, it can be observed in Fig. 2(a) that the sound absorption coefficient is correctly estimated for both normal and oblique incidence. This is expected since the source, which is far from the sensors and the surface can be approximated with a plane wave. The figure also illustrates the inherent deviation that exists between the LR and NLR assumptions. Indeed, the two-surface models are equivalent at normal incidence and diverge as the angle of incidence or the frequency increases (Allard, 1993).

When the source is positioned closer to the sensors and the surface, as shown in Fig. 2(b), an overestimation of the sound absorption coefficient is observed for the WS technique at low frequencies. This overestimation arises from the plane wave assumption, which does not account for the spatial spread of energy in the spherical wave field, as reported in Atalla *et al.* (2006).

In the case of low source heights, inducing a spherical wave field, it is convenient to use the ISM propagation matrix, Eq. (9), instead of the WS technique, in order to account for the spherical spreading of energy. Figure 3(a) shows the sound absorption coefficient at  $0^\circ$  and  $42^\circ$  for a source at  $(0, 0.7 \sin \theta, 0.7 \cos \theta) \text{ m}$ . The estimation is performed using the WS technique and the ISM with a generated pressure field from the Allard *et al.* (1992) model.

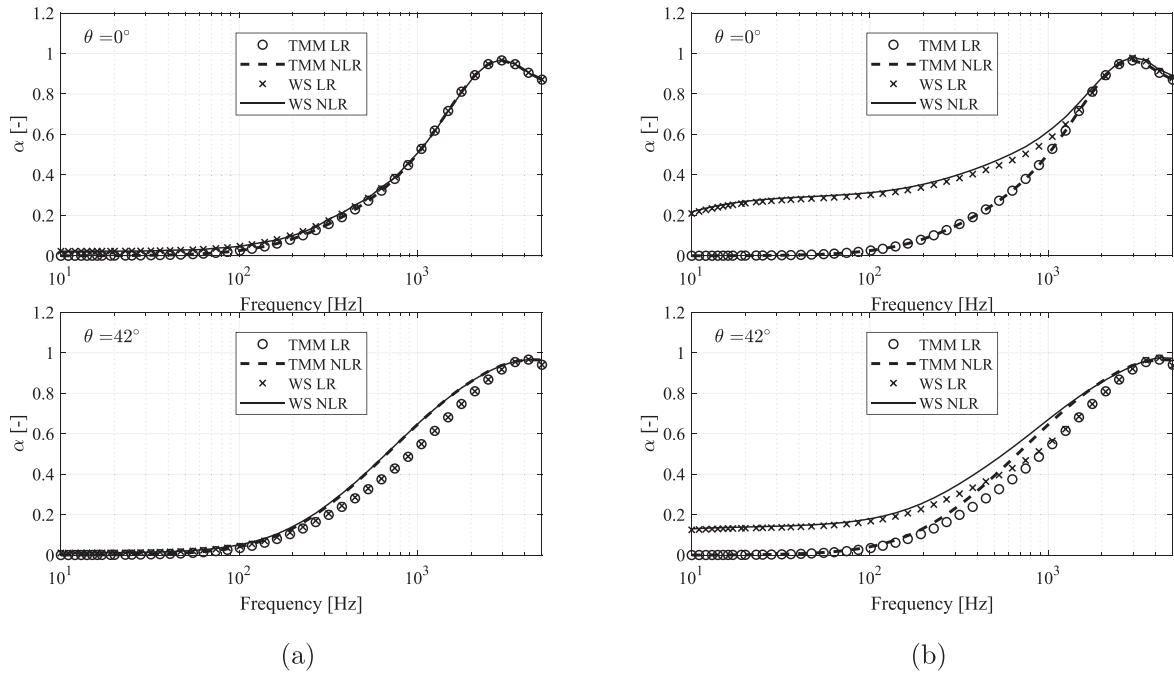


FIG. 2. Sound absorption coefficient at  $0^\circ$  and  $42^\circ$  for a melamine foam with source at (a)  $(0, 10 \sin \theta, 10 \cos \theta)$  m and (b)  $(0, 0.7 \sin \theta, 0.7 \cos \theta)$  m obtained using the TMM and the WS technique method for both LR and NLR assumptions.

The problem is simulated in the presence of Gaussian noise with a fixed amplitude representing background noise. Results are compared with the TMM NLR.

It can be noticed in Fig. 3(a) that while the WS technique overestimates the sound absorption coefficient, the ISM underestimates it. For frequencies below 400 Hz, the estimated absorption using the ISM shows negative values.

negative values occur because the sound absorption coefficient is estimated using a plane wave reflection coefficient that does not account for the spherical energy spread. While iterative techniques have been proposed to attempt to correct for this effect (Brandão *et al.*, 2015), the purpose here is to examine the limitations of a direct retrieval technique as a basis for the interpretation of the experimental results.

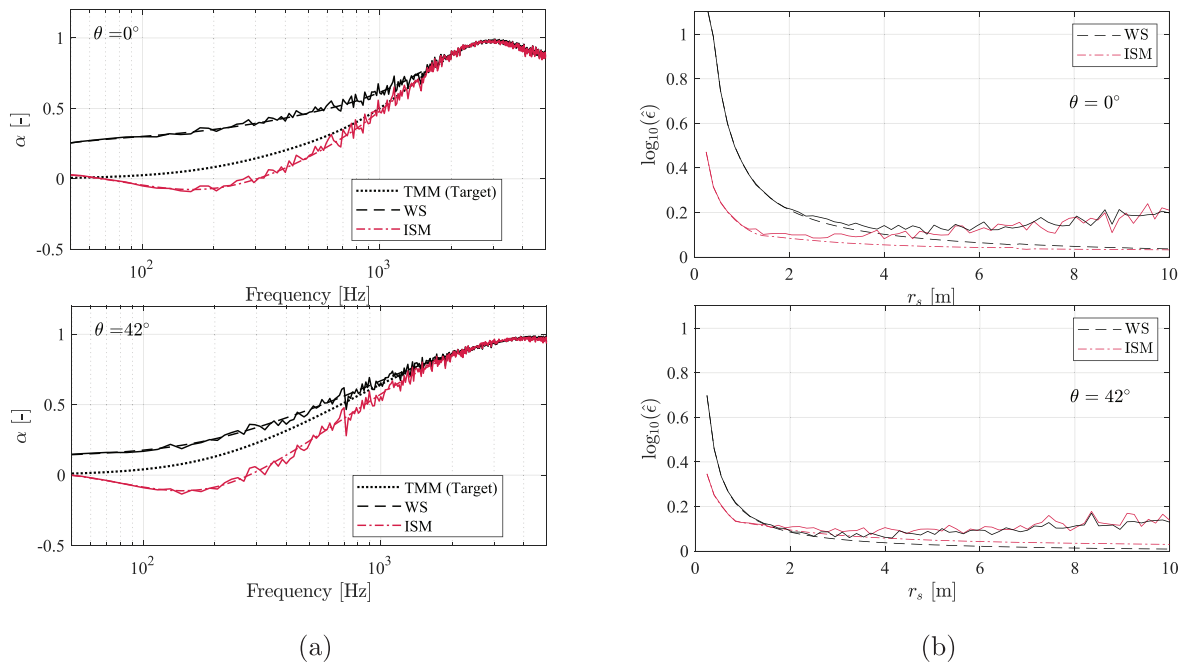


FIG. 3. (Color online) (a) Sound absorption coefficient at  $0^\circ$  and  $42^\circ$  for a melamine foam with source at  $(0, 0.7 \sin \theta, 0.7 \cos \theta)$  m obtained using the TMM NLR, the WS technique, and the ISM with a generated pressure field from the Allard *et al.* (1992) model and (b) averaged error as a function of the distance from the source to the origin; full lines with added background noise on the microphone pressure signals.

Figure 3(b) shows the averaged relative error as a function of the source position, defined as

$$\hat{\epsilon}(\mathbf{r}_s) = \frac{1}{N} \sum_{n=1}^N \frac{|\alpha_{\text{TMM}}(\theta, \omega_n) - \alpha(\mathbf{r}_s, \omega_n)|}{|\alpha_{\text{TMM}}(\theta, \omega_n)|}, \quad (12)$$

where  $\alpha$  is the sound absorption coefficient computed from either the WS technique or the ISM for a source located at  $\mathbf{r}_s = (r_s, \theta)$ .

It can be observed in Fig. 3(b) that the ISM has a smaller error than the WS for  $\theta = 0^\circ$ . Furthermore, the discrepancies between the predictions by the two methods decrease as the distance from the source increases. For this particular case, the retrieval errors for the two models are comparable above 7 m. For the oblique incidence case  $\theta = 42^\circ$ , the averaged error for both methods is reduced and becomes comparable at lower source distances. The error curves without additive noise on the microphone pressure signals illustrate the asymptotic equivalence of the WS and ISM formulations for large source distances. The presence of noise leads to an increase in the retrieval error with large source distances and illustrates the limitations of placing the source far from the sample in a real scenario.

In summary, when the source is placed close to the surface, the ISM can estimate the sound absorption coefficient more accurately, even though both methods do not retrieve perfectly the target sound absorption coefficient. The two methods, in fact, act as lower and upper bounds for the estimated sound absorption coefficient. For far-field sources, both WS and ISM models yield comparable absolute errors.

### B. Robustness of the method for a compact microphone array

This section evaluates the benefits of increasing the number of microphones in the array, in light of the simplified models used for the sound absorption estimation. In particular, the sensitivity of the estimated sound absorption coefficient to uncertainties in the microphone positions given the increase in array spatial extent is investigated.

The sound absorption coefficient is here estimated using the ISM on a pressure field simulated by means of the Allard *et al.* (1992) model with source position at (0, 0, 0.7) m above the melamine foam sample. The core of the microphone array consists of two microphone layers, with a nominal distance from the sample of 0.018 and 0.038 m respectively, similar to the previous section. An optional third layer is placed at 0.058 or 0.0704 m in order to achieve regular or irregular spacing, respectively. For all three configurations, the number of microphones per layer is varied. The additional columns of microphones are added on the y-axis with a regular spacing of 0.04 m. Figure 4 (top) shows the microphone positions for the irregular configuration up to the eighth column.

In order to evaluate the influence of the uncertainty in the microphone positions on the estimated sound absorption coefficient, a Monte Carlo routine is implemented with 1000

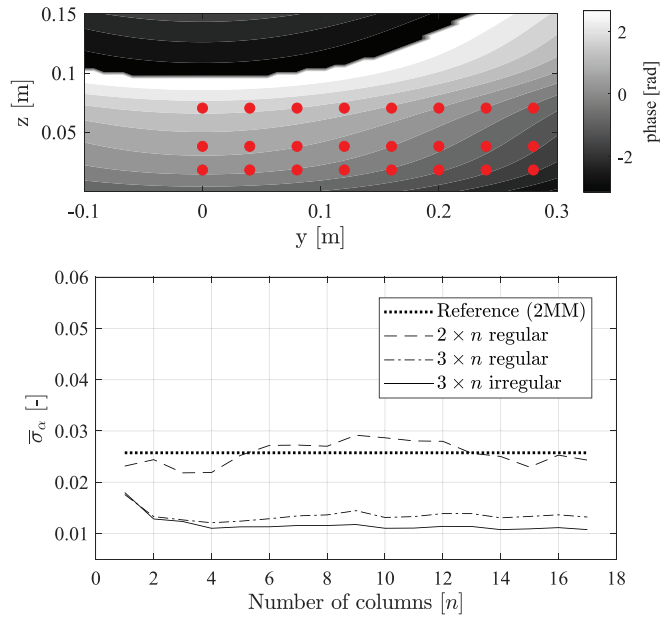


FIG. 4. (Color online) (Top) Pressure field at 2 kHz generated using Allard *et al.* (1992) model above an irregular microphone array and a NLR melamine foam sample; (bottom) average standard deviation of the sound absorption coefficient estimated using the ISM as a function of the number of columns of microphones for a  $2 \times n$ ,  $3 \times n$  regular and irregular microphone array; the standard deviation for the 2MM estimation is shown as a reference.

runs for each scenario (i.e., each configuration and for each additional column). The microphone coordinates are drawn from a normal distribution about their nominal coordinates, using a standard deviation of 1.6 mm. This value was obtained by measuring the coordinates of all microphones in the array of Sec. V A using a digital caliper. As a measure of the sensitivity to microphone position uncertainty, the standard deviation  $\sigma_z$  of the sound absorption coefficient is evaluated over the Monte Carlo runs. This standard deviation is then averaged over the observed frequency range and denoted  $\bar{\sigma}_z$ . Figure 4 (bottom) shows this quantity for the different microphone array configurations. In the figure, the value for the 2MM is used as a reference since the number of microphone columns does not change. The three-layer arrays show close to 50% reduction in sensitivity to microphone position uncertainty, compared with a two-layer array. This is due to the larger number of microphones since their positions are drawn from a normal distribution. The two-layer array with a single column exhibits a sensitivity comparable to that of the 2MM. Similarly for the three-layer configuration, adding microphone columns reduces the uncertainty but no improvement is observed beyond six columns. The reason behind the uncertainty remaining constant above a given number of microphone columns is that the proposed method relies on a rather simplistic propagation model, which does not account for the complexity of the wavefront over larger scales, for instance, as simulated here using the Allard *et al.* (1992) model as input data. Furthermore, the irregular vertical spacing exhibits a small but systematic improvement with respect to the regular layer

spacing. In summary, from an array design standpoint, a three-layer array with irregularly-spaced microphones in the direction normal to the sample can reduce the uncertainty compared to a two-layer configuration, and adding more microphones parallel to the sample has a marginal improvement beyond three columns.

## V. EXPERIMENTAL VALIDATION

In this section, the proposed approach is investigated experimentally using a three-layer microphone array configuration. In Sec. VA, a regular vertical spacing array is examined in terms of sensitivity to errors in the sensor’s positioning similarly to Sec. IVB. The WS technique is applied. In Sec. VB, experimental results for a melamine foam and a gravel sample measured with an irregular array are shown and discussed. In an attempt to improve the low-frequency sound absorption estimation, the ISM is applied. In both subsections, the inversion of the propagation matrix is regularized (Hansen, 1994).

### A. $3 \times n$ microphone array with regular vertical spacing

The microphone array, as shown in Fig. 5, consists of double-layer regularly spaced microphones that are measured at two consecutive heights. The array is constructed in such a way that multiple angles of incidence can be retrieved for a single source position, given that the surface

behaves as locally reactive. In the case of non-locally reactive surfaces, measurements at different source positions are required to retrieve the sound absorption at multiple angles of incidence. Additional microphone layers can improve the estimation in terms of spatial resolution and phase errors (Hald, 2009). However, a compact microphone array setup is desirable in many situations and, in general, it translates to a less cumbersome measurement setup.

The measurement campaign is performed in a silent room with a microphone array above a melamine foam sample as shown in Fig. 5. The setup consists of 34 1/4 in. G.R.A.S. microphones arranged in two layers of 17 microphones each, spaced 0.04 m horizontally and 0.02 m vertically. The layout of the array is chosen so as to horizontally replicate the classical two-microphone setup. The melamine foam sample has a nominal thickness of 0.03 m and a surface area of  $2.14 \times 1.56 \text{ m}^2$ . The measurements are performed with a Simcenter Mid-High-frequency volume velocity source (Q-MHF) fixed at a height of  $0.7 \pm 0.005 \text{ m}$  from the ground. The source is driven by a white noise. The microphone signals are sampled at 25.6 kHz, with a frequency resolution of 1.5625 Hz. Two-hundred averages are performed, using a 50%-overlap Hann window. The measurement is done at 0.1 m and 0.12 m heights, as measured from the surface to the lower layer of microphones, effectively producing a three-layer array with heights at 0.1, 0.12, and 0.14 m. The non-simultaneous acquisition can induce variability and uncertainty in the estimated

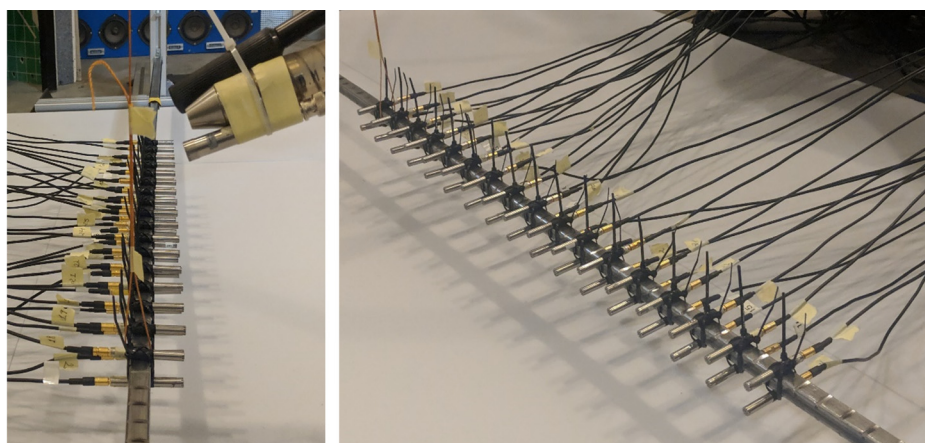
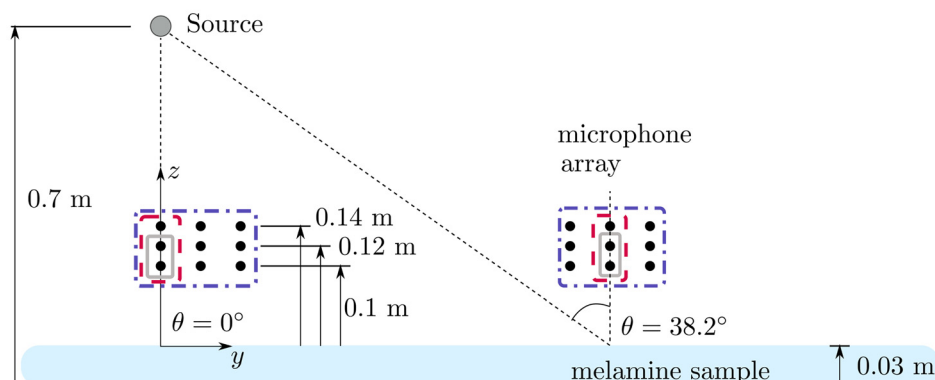


FIG. 5. (Color online) (Top) Setup with a regular-spaced two-layer grid measured at two heights and a monopole source located above the first column and melamine sample; (bottom) schematic of the setup with three layers at two measurement positions (i.e., angle of incidence).



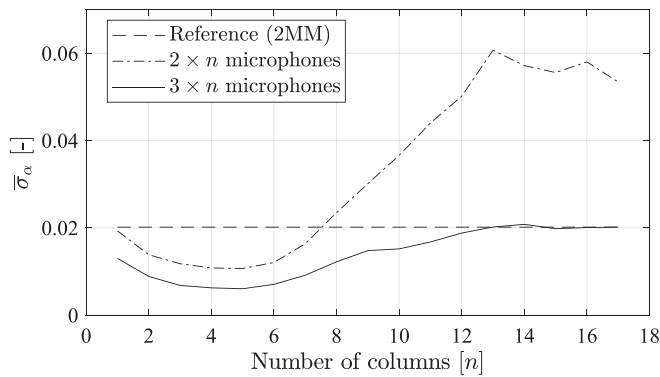


FIG. 6. Frequency averaged standard deviation of the sound absorption coefficient at normal incidence as a function of the number of microphone columns; estimations derive from the WS technique with  $2 \times n$  and with  $3 \times n$  microphone arrays with regular vertical spacing; the standard deviation for the 2 MM estimation is shown as reference.

absorption. Hence, a fixed microphone is used as a phase reference.

Due to the low source power at lower frequencies, the not fully anechoic room and the finiteness of the sample, the results at those frequencies are not considered in the analysis.

Similar to Sec. IV B, a Monte Carlo routine is used to estimate the sensitivity of the estimated sound absorption coefficient to uncertainties in the microphone coordinates. A total of 1000 runs are computed for each configuration and additional column. The microphone coordinates are drawn from a normal distribution about their nominal positions using a standard deviation of 1.6 mm.

Figure 6 shows the averaged standard deviation of the estimated normal incidence sound absorption coefficient, considering the configuration with two-layers ( $2 \times n$  microphones) and three-layers ( $3 \times n$  microphones) for  $n$ -columns

of microphones along the horizontal direction. The results are compared to the standard deviation from the 2 MM, used as reference.

Overall, the  $2 \times n$  microphone array shows higher values for the averaged standard deviation than the  $3 \times n$  microphone array with similar reasoning as in the simulated case from Sec. IV B. It can be observed that the uncertainty in the estimated sound absorption coefficient for both two- and three-layer arrays reaches a minimum value for measurements with 3 to 6 microphone columns. In the three-layer array case, adding more columns of microphones in the estimation results in a slight increase in the averaged standard deviation up to a level similar to the uncertainty of the 2 MM. This increase can be attributed to the spatial extent of the microphone array, over which the simplified model does not account for the actual geometry of the wavefront. In the present case, this highlights the redundancy of sensors, which is sought to be minimized. It is worth noting that the optimum number of columns obtained in Fig. 6 cannot be considered as a general result for other scenarios as it depends on the source position and the sparsity of the microphone array. In general, however, larger source-surface distances allow relaxing the maximum number of microphones to be used.

To further confirm results from Fig. 6, Fig. 7 shows the estimated sound absorption coefficient and its standard deviation due to the uncertainty in microphone positions for a  $2 \times 1$ , a  $3 \times 1$  and a  $3 \times 3$  microphone array. Results are shown for normal incidence in Fig. 7(a) and, for a  $38.2^\circ$  oblique incidence in Fig. 7(b) in accordance with Fig. 5. The  $2 \times 1$  array configuration has microphones positioned at coordinates (0, 0, 0.1) m and (0, 0, 0.12) m. The  $3 \times 1$  array configuration has an additional microphone at (0, 0, 0.14) m and the  $3 \times 3$  microphone array configuration uses the

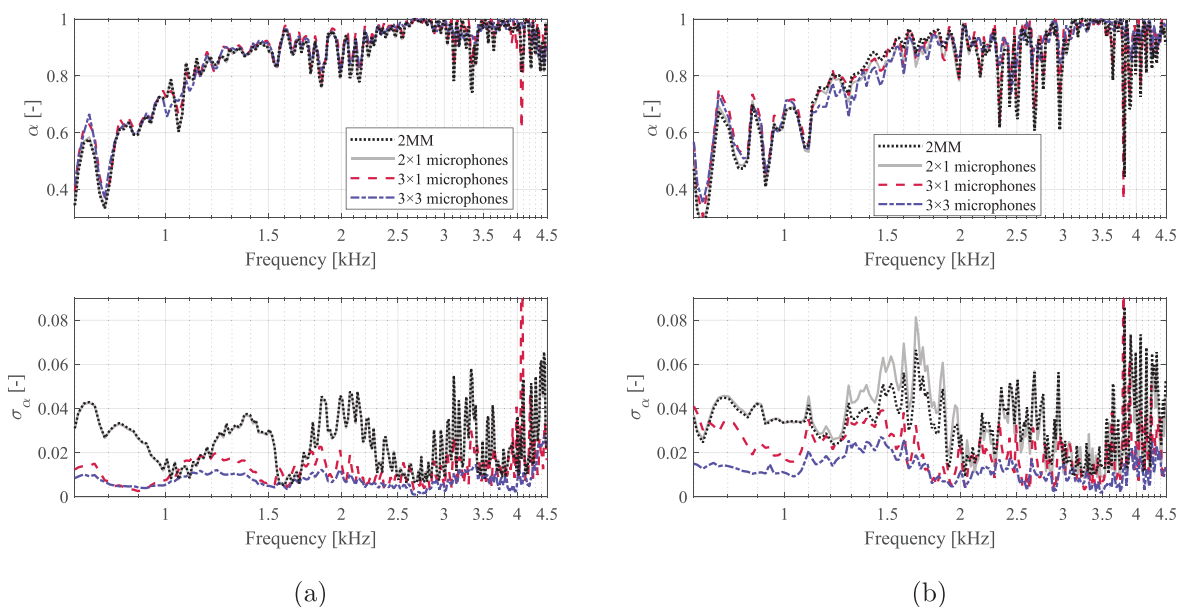


FIG. 7. (Color online) (Top) Nominal value of the estimated sound absorption coefficient using the WS technique for (a) normal incidence and (b) oblique incidence ( $38.2^\circ$ ), (bottom) standard deviation on the estimated sound absorption coefficient for  $2 \times 1$ ,  $3 \times 1$ , and  $3 \times 3$  microphones array configuration and the 2 MM.

previous three microphones with two adjacent columns in the array. In the normal incidence case, the  $3 \times 3$  array has a nonsymmetrical configuration, with two columns on the right side, as indicated in Fig. 5.

To estimate the sound absorption coefficient at oblique incidence, the WS technique is constructed at a new position on the surface of the sample by translating the origin of the Cartesian system to a new position on the surface. In this investigation, to achieve an approximated angle of incidence of  $38.2^\circ$ , the origin is translated 0.52 m away along the y axis to a new origin position. For this angle of incidence, the column closer to this point is column 14 (located at 0.52 m on the y-axis), which is shown in Fig. 5.

In the normal incidence case, the sound absorption coefficient estimated using the WS technique is in agreement with the 2 MM. The small deviations observed, especially at frequencies below 1.4 kHz, can be attributed to the nominal microphone distance not matching precisely the actual position and low signal-to-noise ratio from unwanted reflections. In terms of uncertainty, the  $2 \times 1$  microphone array and the 2 MM show a higher standard deviation compared to the other arrays. Accordingly, as the number of microphones increases, the uncertainty in the estimated sound absorption coefficient decreases.

In the oblique incidence case, a similar behavior to that in the normal incidence is observed. Note that at frequencies between 1.3 and 2 kHz, the 2 MM provides lower uncertainty estimations than the WS technique with a  $2 \times 1$  microphone array. This can be attributed to the finite ensemble of runs in the Monte Carlo routine. Similar to the normal incidence case, with additional microphones, the WS technique is capable of reducing significantly the uncertainty for an oblique-incidence sound absorption coefficient estimation as seen for both  $3 \times 1$  and  $3 \times 3$  microphone arrays.

Figure 8 shows the sound absorption coefficient against the angle of incidence for three arbitrarily chosen frequencies. The measurements are compared with the TMM using a LR model where the melamine foam parameters are the same as Sec. IV. The maximum obtained angle of incidence is determined by the source-surface distance and microphone array spatial extent. A good agreement can be observed overall, with the  $2 \times 1$  array exhibiting higher variability than the other configurations and the  $3 \times 3$  array showing both a low variability and a closer match with the TMM prediction.

In summary, the measurements with a regular vertical microphone spacing array show that a three-layer configuration is beneficial in terms of reducing uncertainty from microphone positions. Furthermore, the results are in good agreement with TMM predictions and provide an improved robustness in comparison with the classical 2 MM. In general, more microphones reduce the uncertainty of the measurements. However, an increase in uncertainty of the estimated sound absorption coefficient arises when the microphone array is spatially extended. This can be attributed to the discrepancy between the measured data and the rather simplistic model here used, which does not capture

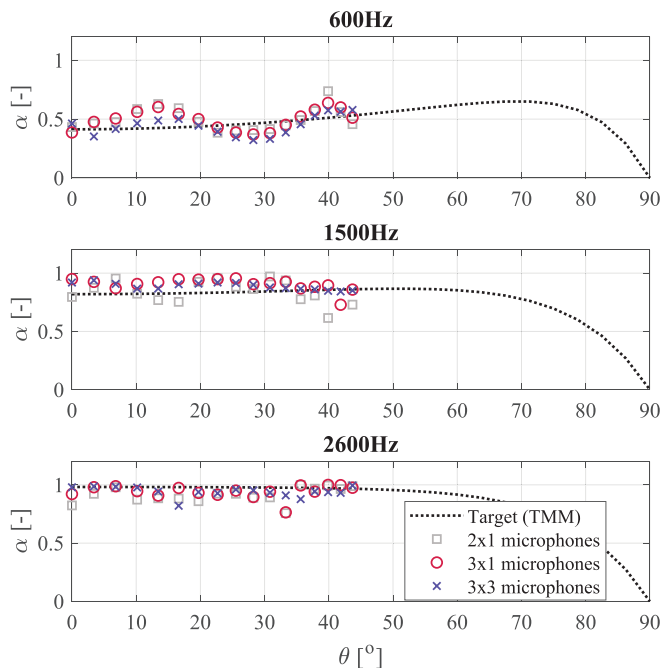


FIG. 8. (Color online) Estimated sound absorption coefficient against the angle of incidence for arbitrarily chosen frequencies. The result is computed using the WS for  $2 \times 1$  microphones,  $3 \times 1$  microphones, and  $3 \times 3$  microphones array configurations; the approach is compared to the TMM with a locally reactive assumption.

the full complexity of the wavefront over larger scales. Therefore, a good compromise is achieved with a  $3 \times 3$  microphone array configuration in the present case. In light of this observation and the results of the numerical validation, a  $3 \times 3$  array with irregular vertical spacing is used in the following.

### B. $3 \times 3$ microphone array with irregular vertical spacing

This section evaluates the performance of a  $3 \times 3$  array with irregular vertical spacing in comparison with the 2 MM. Contrary to the measurements in Sec. VA, here all microphone signals are acquired simultaneously. The measurement setup is shown in Fig. 9. The monopolar source is placed at a height of  $0.687 \pm 0.005$  m from the ground and moved horizontally to various positions to achieve different angles of incidence. The measurements are performed using the Simcenter Q-sources low-frequency volume velocity monopolar source (Q-MED) with better low-frequency performance than the Q-MHF. The source is driven by a pink noise. The microphone signals are sampled at 25.6 kHz, with a frequency resolution of 6.25 Hz. 300 averages are performed, using a 50%-overlap Hann window. Two samples are tested using the  $3 \times 3$  microphone array, the melamine foam presented in Sec. VA and a gravel sample. The gravel sample has a nominal thickness of 0.045 m and a surface area of  $0.85 \times 0.55$  m<sup>2</sup> as shown in Fig. 9 (center). The microphone coordinates are provided in Table I for the melamine foam sample. In the case of the gravel sample, the array is 4 mm closer to the sample. The microphone

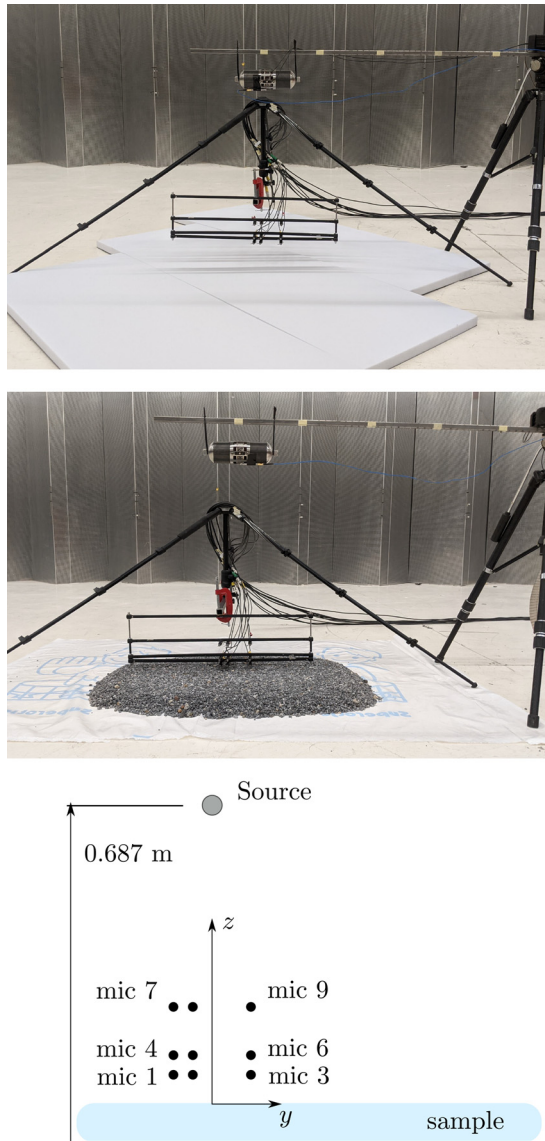


FIG. 9. (Color online) Measurement setup of the  $3 \times 3$  irregularly spaced microphone array above a (top) melamine foam, (center) a gravel sample, and (bottom) schematic with microphone configuration, source, and sample position in terms of the origin of the coordinate system.

coordinates are with respect to the surface of the sample and following the ordering convention of Fig. 9 (bottom).

The equivalent fluid parameters of the gravel sample are obtained by performing an inverse estimation on measurements with a vertical two-microphone impedance tube. The latter has a diameter of 0.1 m and contains two 1/2 in. G.R.A.S. microphones at positions 10.795 and 19.05 cm with respect to the tube opening. The impedance tube measurements are valid up to 1.97 kHz in room temperature

TABLE I. Coordinates of microphone array in the  $x = 0$  plane above the melamine foam sample.

Mic #	1	2	3	4	5	6	7	8	9
y (cm)	-5.1	-2.7	5.0	-5.3	-2.6	4.9	-5.1	-2.6	5.0
z (cm)	1.7	1.6	1.8	3.6	3.6	3.7	8.7	8.8	9.0

conditions (ISO, 2010). Three gravel samples with different thicknesses are measured and the inverse estimation is performed using the three measurements simultaneously (Cuenca *et al.*, 2021). The parameters obtained are: porosity  $\phi = 0.20$ , flow resistivity  $\sigma = 7798 \text{ Pa} \cdot \text{s} \cdot \text{m}^{-2}$ , tortuosity  $\alpha_\infty = 1.32$ , viscous characteristic length  $\Lambda = 224 \mu\text{m}$ , thermal characteristic length  $\Lambda' = 449 \mu\text{m}$ .

Figure 10 shows the estimated sound absorption coefficient for the melamine foam sample at  $0^\circ$ ,  $17^\circ$ ,  $32^\circ$ , and  $42^\circ$  angle of incidence. Since the source is positioned relatively close to the surface, the ISM is selected to estimate the sound absorption coefficient. For comparison, an estimation of the sound absorption coefficient is drawn from simulated data, obtained by generating the pressure field at the microphone locations using the Di and Gilbert (1993) model from Sec. II B. The target sound absorption coefficient is computed using the TMM with a LR assumption and the equivalent fluid parameters given in Sec. IV.

Additionally, the 2MM using Eq. (11) is shown for comparison. The two microphones used in the 2MM are the first two layers of the middle column, i.e., microphones 2 and 5 (refer to Fig. 9, bottom, and Table I).

It can be observed in Fig. 10 that the estimated absorption from the measurements is in good agreement with the other methods. Compared with the 2MM, the proposed microphone array shows better results at frequencies below 700 Hz. Compared with the target value, an underestimation and negative values are retrieved in the lower frequencies. This is expected because the ISM does not account for the diffraction effects and the sound absorption coefficient is estimated using a plane wave sound absorption coefficient, as discussed in Sec. IV A. Nonetheless, the measurement results are in good agreement with the results obtained from the simulated pressure field. The differences between the simulated and estimated sound absorption coefficients below 1.3 kHz are consistent with the finite-size effect (Hald *et al.*, 2019), as the Di and Gilbert (1993) model is an infinite sample model. In addition, the differences below 100 Hz can be exacerbated by the ill-conditioning of the propagation matrix. In terms of angle of incidence, there is not a considerable variation of absorption behavior, which is expected for a homogeneous melamine foam sample.

Figure 11 shows the estimated sound absorption coefficient for the gravel sample. The simulated absorption is computed similarly to the previous case. In this case, the Allard *et al.* (1992) model from Sec. II C is preferred, as the latter captures the shift of the absorption peak due to the non-locally reactive behavior. A good agreement of the estimated absorption is obtained for frequencies above 1 kHz for both methods. In particular, the angle-dependent frequency of the absorption peak closely follows the numerical prediction. At lower frequencies, the effect of sample size plays a major role as it causes a dip in the absorption around 700 Hz in the normal incidence case. Nevertheless, as in the case of the melamine foam sample, the proposed method using a compact microphone array shows a clear improvement with respect to the 2MM.

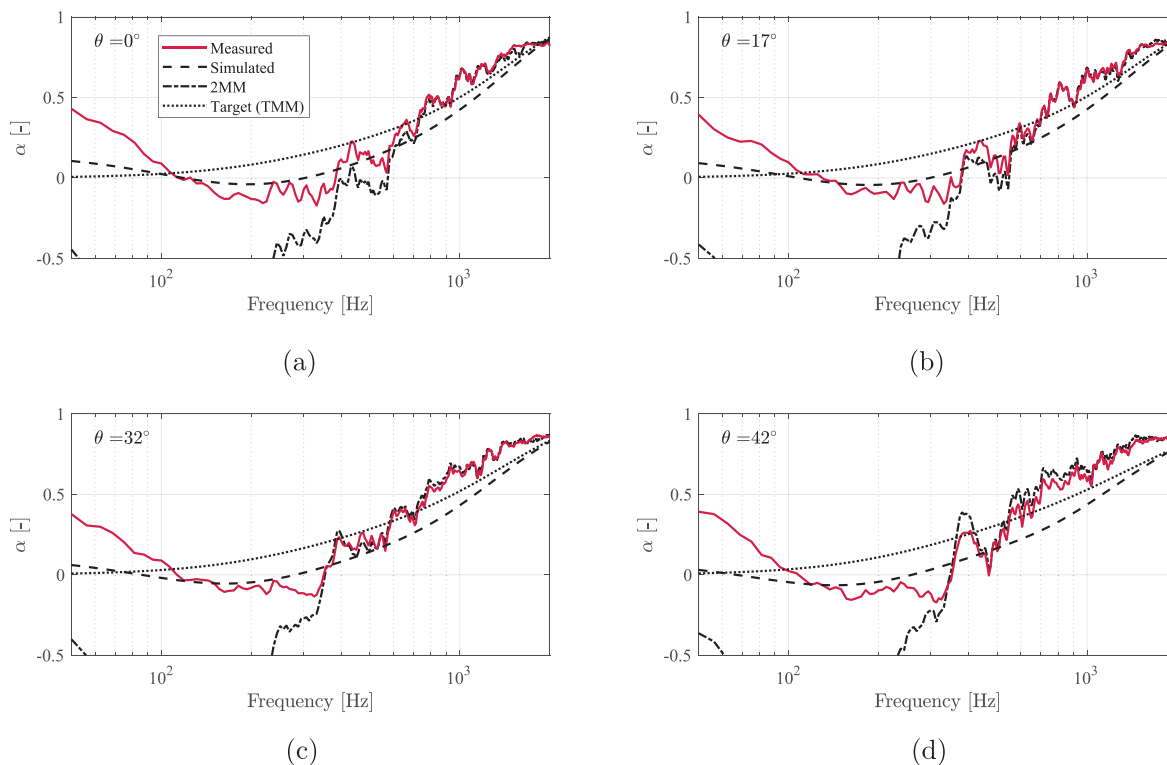


FIG. 10. (Color online) Estimated sound absorption coefficient at (a)  $0^\circ$ , (b)  $17^\circ$ , (c)  $32^\circ$ , and (d)  $42^\circ$  for a melamine foam sample using ISM and simulated pressure field based on the [Di and Gilbert \(1993\)](#) model.

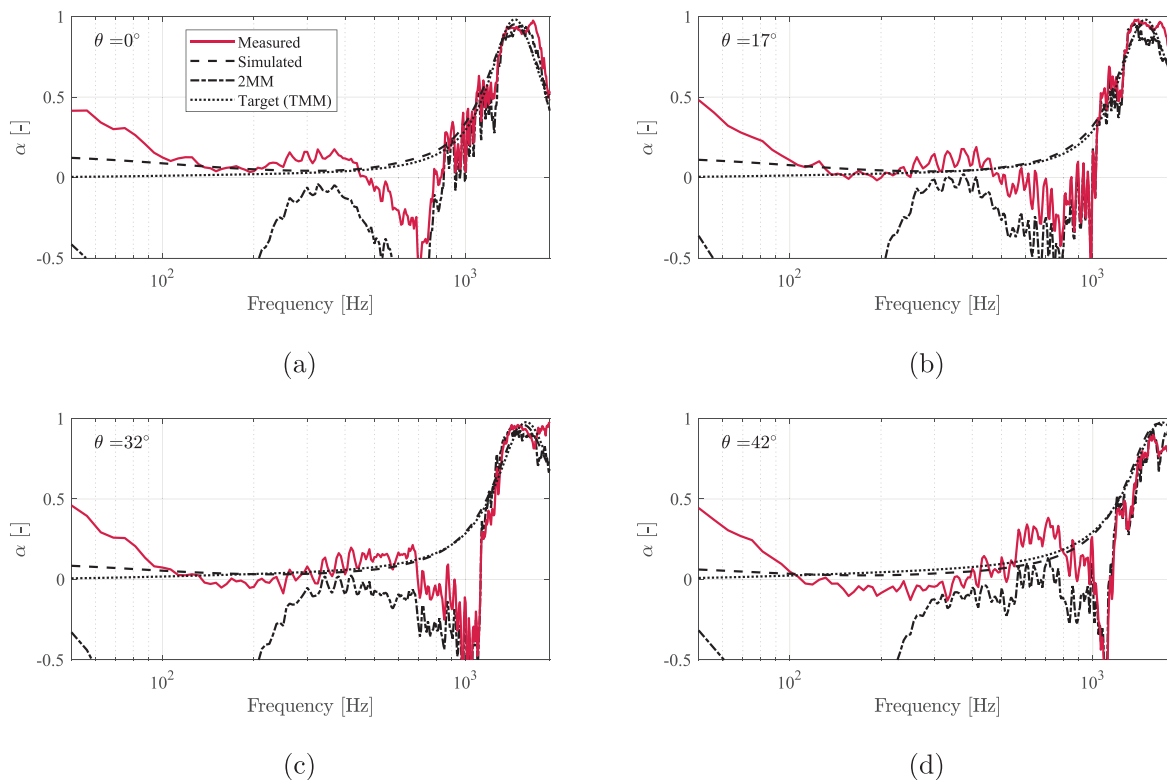


FIG. 11. (Color online) Estimated sound absorption coefficient at (a)  $0^\circ$ , (b)  $17^\circ$ , (c)  $32^\circ$ , and (d)  $42^\circ$  for a gravel sample using ISM and simulated pressure field based on the [Allard et al. \(1992\)](#) model.

## VI. CONCLUSION

This paper proposes a method for estimating the sound absorption coefficient by inverting a model of the propagation field using both the WS technique and the ISM. The main goal is to improve the estimated absorption coefficient by introducing modifications to the classical two-microphone setup such as an added microphone layer, irregular spacing in the normal direction, and additional microphone columns while keeping compact dimensions for portability reasons. It is worth noting that given this constraint, other design variables such as the microphone spacing itself are outside the scope of this work. The method was numerically validated against the transfer matrix method and the classical two-microphone method for both locally and non-locally reactive surface models. An uncertainty analysis showed a  $3 \times 3$  irregularly-spaced microphone array to exhibit the desired capabilities while retaining a compact design. Experimental results on melamine foam and gravel samples show a clear improvement over the classical two-microphone method, in particular providing better reliability at low frequencies and overall robustness, despite the array compactness. As the estimation relies on very simple models, i.e., a pair of plane waves or point sources, the performance of the method is affected by the inability to capture the full complexity of the wave field. In addition, the finite-size effect of the samples affects the estimations as it is not addressed in the present work.

Further improvements in the estimation can potentially be achieved by including scattering and diffraction in the propagation matrix as in the third term of the Allard *et al.* (1992) or Di and Gilbert (1993) models. Additional improvements can also be achieved by using a more realistic propagation model or by increasing the number of waves, e.g., using a wave decomposition approach, however, at the expense of increasing the number of microphones (Nolan, 2020; Richard and Fernandez-Grande, 2019).

## ACKNOWLEDGMENTS

We gratefully acknowledge the European Commission for its support of the Marie Skłodowska Curie program through the H2020 ETN PBNv2 project (GA 721615). Special thanks to Dr. Giulio Dolcetti, at the University of Sheffield, for the measurements of the uncertainty in the microphone positions and Professor Christ Glorieux, at KU Leuven, for providing the melamine foam samples. The authors would also like to thank the three anonymous reviewers for their valuable comments and suggestions that greatly improved the manuscript.

Alkmim, M., Bianciardi, F., Vandernoot, G., De Ryck, L., Cuenca, J., and Janssens, K. (2020). "Pass-by noise synthesis from transfer path analysis using IIR filters," in *Vibration Engineering for a Sustainable Future* (Springer, New York).

Allard, J. F. (1993). *Propagation of Sound in Porous Media: Modelling Sound Absorbing Materials* (Springer, Amsterdam, the Netherlands).

Allard, J.-F., and Champoux, Y. (1989). "In situ two-microphone technique for the measurement of the acoustic surface impedance of materials," *Noise Control Eng. J.* **32**(1), 15–23.

Allard, J.-F., Lauriks, W., and Verhaegen, C. (1992). "The acoustic sound field above a porous layer and the estimation of the acoustic surface impedance from free-field measurements," *J. Acoust. Soc. Am.* **91**(5), 3057–3060.

Atalla, N., Sgard, F., and Amedin, C. K. (2006). "On the modeling of sound radiation from poroelastic materials," *J. Acoust. Soc. Am.* **120**(4), 1990–1995.

Bezemer-Krijnen, M., Wijnant, Y. H., Boer, A. D., and Bekke, D. (2014). "On the sound absorption coefficient of porous asphalt pavements for oblique incident sound waves," in *Proceedings of Internoise*, November 16–19, Melbourne, Australia, p. 7.

Brandão, E., Lenzi, A., and Paul, S. (2015). "A review of the *in situ* impedance and sound absorption measurement techniques," *Acta Acust. united Ac.* **101**(3), 443–463.

Champoux, Y., and Allard, J.-F. (1991). "Dynamic tortuosity and bulk modulus in air-saturated porous media," *J. Appl. Phys.* **70**(4), 1975–1979.

Cuenca, J., and De Ryck, L. (2015). "In-situ sound absorption of ground surfaces: Innovative processing and characterisation methods," in *Proceedings of Euronoise*, May 31–June 3, Maastricht, Germany, p. 6.

Cuenca, J., Göransson, P., De Ryck, L., and Lähivaara, T. (2021). "Deterministic and statistical methods for the characterisation of poroelastic media from multi-observation sound absorption measurements," *Mech. Syst. Signal Process.* **163**, 108186.

Di, X., and Gilbert, K. E. (1993). "An exact Laplace transform formulation for a point source above a ground surface," *J. Acoust. Soc. Am.* **93**(2), 714–720.

Dupont, S., Melon, M., and Berry, A. (2020). "Characterization of acoustic material at oblique incidence using a spherical microphone array," *J. Acoust. Soc. Am.* **147**(5), 3613–3625.

Hald, J. (2009). "Basic theory and properties of statistically optimized near-field acoustical holography," *J. Acoust. Soc. Am.* **125**(4), 2105–2120.

Hald, J., Song, W., Haddad, K., Jeong, C.-H., and Richard, A. (2019). "In-situ impedance and sound absorption coefficient measurements using a double-layer microphone array," *Appl. Acoust.* **143**, 74–83.

Hansen, P. C. (1994). "Regularization tools: A Matlab package for analysis and solution of discrete ill-posed problems," *Numer. Algorithms* **6**(1), 1–35.

ISO (1998). ISO 10534-2, *Acoustics—Determination of Sound Absorption Coefficient and Impedance in Impedance Tubes—Part 2: Transfer-Function Method* (ISO, Geneva, Switzerland).

ISO (2003). ISO 354, *Acoustics—Measurement of Sound Absorption in a Reverberation Room* (ISO, Geneva, Switzerland).

ISO (2010). ISO 13472-2, *Acoustics — Measurement of Sound Absorption Properties of Road Surfaces In Situ — Part 2: Spot Method for Reflective Surfaces* (ISO, Geneva, Switzerland).

ISO (2014). ISO 10844, *Acoustics — Specification of Test Tracks for Measuring Noise Emitted by Road Vehicles and Their Tyres* (ISO, Geneva, Switzerland).

ISO (2015). ISO 362-1, *Measurement of Noise Emitted by Accelerating Road Vehicles – Engineering Method – Part 1: M and N Categories* (ISO, Geneva, Switzerland).

Johnson, D. L., Koplik, J., and Dashen, R. (1987). "Theory of dynamic permeability and tortuosity in fluid-saturated porous media," *J. Fluid Mech.* **176**, 379–402.

Kim, Y., and Nelson, P. (2004). "Optimal regularisation for acoustic source reconstruction by inverse methods," *J. Sound Vib.* **275**(3–5), 463–487.

Nelson, P., and Yoon, S. (2000). "Estimation of acoustic source strength by inverse methods: Part I, conditioning of the inverse problem," *J. Sound Vib.* **233**(4), 639–664.

Nolan, M. (2020). "Estimation of angle-dependent absorption coefficients from spatially distributed *in situ* measurements," *J. Acoust. Soc. Am.* **147**(2), EL119–EL124.

Ottink, M., Brunskog, J., Jeong, C.-H., Fernandez-Grande, E., Trojgaard, P., and Tiana-Roig, E. (2016). "In situ measurements of the oblique incidence sound absorption coefficient for finite sized absorbers," *J. Acoust. Soc. Am.* **139**(1), 41–52.

Rathsam, J., and Rafaely, B. (2015). "Analysis of absorption *in situ* with a spherical microphone array," *Appl. Acoust.* **89**, 273–280.

Richard, A., and Fernandez-Grande, E. (2019). "Comparison of two microphone array geometries for surface impedance estimation," *J. Acoust. Soc. Am.* **146**(1), 501–504.

Richard, A., Fernandez-Grande, E., Brunsog, J., and Jeong, C.-H. (2017). "Estimation of surface impedance at oblique incidence based on sparse array processing," *J. Acoust. Soc. Am.* **141**(6), 4115–4125.

Robin, O., Berry, A., Doutres, O., and Atalla, N. (2014). "Measurement of the sound absorption coefficient of sound absorbing materials under a synthesized diffuse acoustic field," *J. Acoust. Soc. Am.* **136**(1), EL13–EL19.

Tamura, M. (1990). "Spatial Fourier transform method of measuring reflection coefficients at oblique incidence. I: Theory and numerical examples," *J. Acoust. Soc. Am.* **88**(5), 2259–2264.

Wang, Y., and Chen, K. (2018). "Sparse plane wave decomposition of a low frequency sound field within a cylindrical cavity using spherical microphone arrays," *J. Sound Vib.* **431**, 150–162.